

# Fabrication of Millimeter-Long Carbon Tubular Nanostructures Using the Self-Rolling Process Inherent in Elastic Protein Layers

Hyojin Ko, Leila F. Deravi, Sung-Jin Park, Jingon Jang, Takhee Lee, Cheong Kang, Jin Seok Lee, Kevin Kit Parker, and Kwanwoo Shin\*

Millimeter-long conducting fibers can be fabricated from carbon nanomaterials via a simple method involving the release of a prestrained protein layer. This study shows how a self-rolling process initiated by polymerization of a micropatterned layer of fibronectin (FN) results in the production of carbon nanomaterial-based microtubular fibers. The process begins with deposition of carbon nanotube (CNT) or graphene oxide (GO) particles on the FN layer. Before polymerization, particles are discrete and nonconducting, but after polymerization the carbon materials become entangled to form an interconnected conducting network clad by FN. Selective removal of FN using high-temperature combustion yields freestanding CNT or reduced GO microtubular fibers. The properties of these fibers are characterized using atomic force microscopy and Raman spectroscopy. The data suggest that this method may provide a ready route to rapid design and fabrication of aligned biohybrid nanomaterials potentially useful for future electronic applications.

In nature, shape change can be achieved via directional stresses induced within intrinsically layered tissues. When tension is released in such tissues, active motions such as coiling,


H. Ko, Prof. K. Shin  
Department of Chemistry and Institute of Biological Interfaces  
Sogang University  
Seoul 04107, South Korea  
E-mail: kwshin@sogang.ac.kr

Prof. L. F. Deravi  
Department of Chemistry and Chemical Biology  
Northeastern University  
Boston, MA 02115, USA

Dr. S.-J. Park, Prof. K. K. Parker  
Disease Biophysics Group  
Wyss Institute for Biologically Inspired Engineering  
John A. Paulson School of Engineering and Applied Sciences  
Harvard University  
Cambridge, MA 02138, USA

Dr. J. Jang, Prof. T. Lee  
Department of Physics and Astronomy  
and Institute of Applied Physics  
Seoul National University  
Seoul 08826, South Korea

C. Kang, Prof. J. S. Lee  
Department of Chemistry  
Sookmyung Women's University  
Seoul 04373, South Korea

 The ORCID identification number(s) for the author(s) of this article can be found under <https://doi.org/10.1002/adma.201701732>.

DOI: 10.1002/adma.201701732

twisting, or bending are generated. Such behaviors are observed in newly growing tendrils of *Cucumis sativus* (cucumber), which curl to release the stress that occurs when a gelatinous part of the tendril lignifies.<sup>[1]</sup> The seed pods of *Bauhinia variegata* twist to form helical structures when strain is applied on them by diagonally oriented fibrous layers, and the pine cones of *Pinus radiata* open their scales according to dissimilar expansion of differently aligned inner and outer cellulose microfibrils.<sup>[2,3]</sup> The stress induced by a mismatch between different layers of tissue gives rise to an interfacial internal strain that, when released, causes a bending motion.<sup>[4–6]</sup>

Inspired by these bending motions in nature, a technique to shape 3D microstructures using the strain-driven self-rolling technique has been developed.<sup>[7–9]</sup> This technique makes use of internal strains that can arise at a heterogeneous interface where two layers of mismatched materials make contact. Examples of microstructures fabricated from such heterogeneous interfaces via the self-rolling technique include capacitors fabricated using mismatched strained layers containing metals, oxides, and semiconductors; bilayered stimuli-responsive polymer hydrogel actuators whose swelling properties are affected by changes in temperature, pH, salt concentration, and light; and tubular structures of cells created from stretched polymeric films on which cells have been cultured.<sup>[10–14]</sup> Strain between different layers can also be generated when a single, often elastic layer is in direct contact with a hard substrate, resulting in a prestrained layer. When the prestrained layer is released from the substrate, a self-rolling motion is generated. So far, only a few examples of self-rolling motion with a single layer have been reported, such as rolled-up tubes with a metal layer or a semiconductor layer.<sup>[15]</sup>

Recently Parker and co-workers reported that protein microfibers could be produced from highly strained patterned protein layers deposited on a substrate by microcontact printing.<sup>[16,17]</sup> Upon release from the substrate, the patterned protein layers formed centimeter-long, highly uniform nanofabrics. We hypothesized that the contracting motions of a prestrained protein layer could be used to induce homogeneous fibrillar structures from nanomaterials deposited on the protein layer. Similar to making a California roll (during which the filling layer that tops the rice layer is compressed into a tube when the rice layer is rolled and pressed), releasing the strain on a protein

layer causes it to roll into a tube along its transverse axis, in the process squeezing the layer of deposited nanomaterials and inducing entanglement and physical contact. We found that strain-driven self-rolling could be used to fabricate carbon nanotube (CNT) or graphene oxide (GO) composite fibers via isotropic loading on the protein pattern before release. When the protein layer is selectively removed by combustion, only the CNT or GO fibers remain, suggesting an unprecedented route to producing conducting carbon fibers. Fabrication of micro- to macroscale architectures of nanomaterials makes it possible to translate nanoscale properties to the macroscale. In particular, CNT and graphene have been commonly used for flexible electronics and smart fabrics because of their flexibility, modulus, and conductivity. Consequently, the production of highly oriented fibrous structures is an important step toward their application. Fibers are much more convenient to use than individual nanoparticles, and intensely packed structures offer higher modulus and conductivity.

To build up the prestrained protein layer, we used microcontact printing ( $\mu$ CP) to deposit a layer of fibronectin (FN) on top of a water-soluble poly(*N*-isopropylacrylamide) (PIPAAm) film (Figure 1) spin-coated onto a glass coverslip.<sup>[16–18]</sup> The printing process yielded a prestrained protein layer of FN on the PIPAAm-coated coverslip. Next, a CNT or GO solution was printed onto the FN layer, producing overlaid carbon structures. When the sample was immersed in warm water that was then cooled below 32 °C, the uncrosslinked PIPAAm layer swelled as the temperature dropped, which released the prestrained FN layers from the substrate and induced the self-rolling process. The composite structure rolled into a dual tubular shape with the CNT or GO particles on the inside and polymerized FN on the outside, to form a protein-carbon microfiber structure. After selective removal of the FN cladding, the CNT or GO microfibers remained as a self-rolled tubular nanostructure. To test whether this self-rolling technique can be applied to nanomaterials beyond CNTs and GO, we demonstrated fabrication of composite fibers containing quantum dots (QDs) (Figure 1b), silver nanoparticles (AgNPs) and nanowires (AgNWs) (Figure 1c,d), and fluorescent microbeads (Figure 1e). In each case, the self-rolling force from the prestrained FN layer was enough to place these nanostructures into a localized configuration, suggesting that our process can be applicable to multiple material geometries. Note that the images in Figure S1 (Supporting Information) confirmed that the tubular fiber structures from QDs, AgNPs, and AgNWs were remained even after the FN removal process. (Figure S1, Supporting Information).

As soon as the prestrained FN layer released from the sacrificial layer in the presence of a low-temperature aqueous solution, it rolled along its transverse axis on both edges (Figure 2a–c; Movie S1, Supporting Information). The simultaneous rolling from both edges produced a 20  $\mu$ m thick dual tubular microstructure that was 100  $\mu$ m wide and 30 mm long (Figure 2). The  $\mu$ CP technique simultaneously produced hundreds of patterned protein layers, and the produced fibers were highly homogeneous. The rolling process was completed within 30 s when the sacrificial layer consisted of PIPAAm. When the sacrificial layer consisted of substances that are readily soluble in water, that is, dextran or sucrose, the process was completed in an even shorter time. This was a relatively quick process

in comparison to other curling processes involving metal or hydrogel layers, indicating that the elastic FN patterns instantly contract upon release.<sup>[11–13,19]</sup>

The instant contraction and subsequent rolling of the FN layer led to rolling of the upper layer of GO or CNT particles, inducing physical contact between the dispersed particles (Figure 2b). Consequently, particle-core tubular structures formed simultaneously with the FN tube, as shown in Figure 2c. At first, the ultrathin layer of CNT or GO was faintly visible on the Alexa Fluor dye-tagged FN layer (Figure 2a), but then the layer became visibly darker as the FN patterns contracted (Figure 2b). As the FN layer contracted, the distance between the dispersed GO particles drew nearer, eventually bringing them into physical contact as the rolling process progressed. The FN/GO double-layered tubular fibers were then incubated in a furnace to selectively burn out the FN cladding. The scanning electron micrograph (SEM) in Figure 2d shows the tubular GO structure that remained after FN removal. The final result was millimeter-long GO microtubules with a dual tubular microstructure. We repeated this process to form CNT microtubules, suggesting that this process can be used to form a millimeter-long fabric from any nanomaterial without complex fabrication steps as long as the nanomaterial can be stamped on top of the FN layer.

Figure 3a shows an atomic force microscopy (AFM) image around the edge of the microcontact-printed FN layer on the glass substrate, showing the sharpness and flatness of the printed layer, which is  $\approx$ 8 nm thick. Studies show that FN molecules adhered to a substrate undergo conformational unfolding to an insoluble extended conformation.<sup>[17,20,21]</sup> Although extracellular matrix (ECM) proteins are thought to provide rigid mechanical strength, individual ECM proteins can be stretched to several times their relaxed length. It has been previously reported that a single FN molecule maintains its elasticity at up to six times of its molecular stretch ( $\lambda$ ) within the fibril. Stretched FN molecules thus yield a large extended random network that acts much like a sheet of stretched rubber. When highly stretched FN molecules are released from a rigid substrate layer, the resulting recoil of the FN network causes the layer to contract and curl. Figure 3b,c shows CNT and GO particles from a dispersed solution overlaid on the FN layer at thicknesses of  $\approx$ 60 and 4 nm, respectively. The dual tubular microstructure of FN/GO fibers is shown in Figure 3d in a 3D reconstructed confocal image that is paired with an SEM image. Cross-sectional SEM images of tubular structures made of FN only, FN/CNT, and FN/GO are shown in Figure 3e–g. A very smoothly sectioned layer is seen in the FN only sample, while the characteristic features of overlaid carbon particles, protruded nanotubes, and multistacked layers are clearly observed in the FN/CNT and FN/GO samples. Note that in all samples shown in the figure the microtubules are hollow.

An advantage of this approach is that one can control the dimensions of tubular structures by the dispersed nanomaterials. As shown in the bright field images in Figure 4a, when we patterned rectangular FN/CNT layers of 40  $\times$  200  $\mu$ m<sup>2</sup> via the  $\mu$ CP technique, highly homogeneous FN/CNT rods of  $\approx$ 150  $\mu$ m long were achieved. Millimeter-length wires were readily obtained when we printed millimeter-long line patterns. Fiber widths were as thin as 10  $\mu$ m, but fiber lengths could

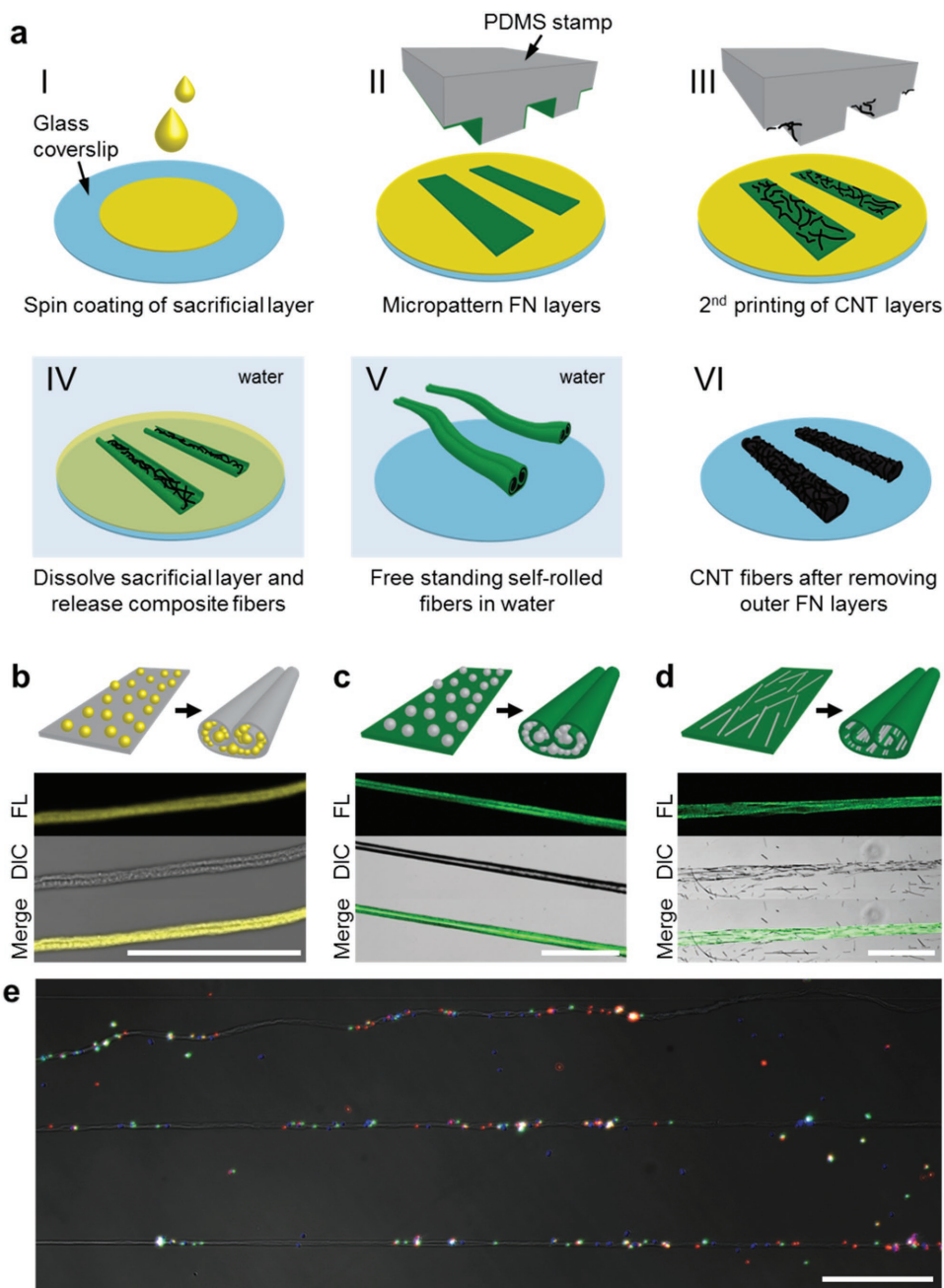


**Figure 1.** Fabrication of fibers using a prestrained protein layer and various nanomaterials. a) Schematic illustration of the fabrication process (I–VI). b) QD incorporated fibers. c) FN/AgNP fibers. d) FN/AgNW fibers. e) Microbead embedded fibers. Confocal fluorescence (FL) images were merged with differential interference contrast (DIC) microscope images (b–e). In case of (b) and (e), FN was not labeled with fluorescent dye for accurate observation of QD and fluorescent microbeads inside fibers. Scale bars are 100  $\mu\text{m}$ .

be extended up to centimeters, as demonstrated in Figure 2b. Mechanical yarning or electrospinning are often used to produce such long carbon-based wires,<sup>[22–24]</sup> but our method produced multiple highly defined wires within just a few seconds, without any complex processing. The diameter of the rods or wires was controlled by the initial width of the FN patterns (Figure 4c). Fiber width increases linearly as pattern size increases, as shown in Figure 4d. Fiber diameter was measured from the confocal image's fluorescence intensity, as explained

in Figure S2 (Supporting Information). The addition of a layer of GO or CNT ( $\approx 4$  and  $\approx 60$  nm height, respectively) cause fabricated fibers to become progressively thicker as the pattern width increased.

Given the natural conductivity of CNT and GO fibers,<sup>[22,25–27]</sup> we next investigated the electrical properties of CNT and GO microtubular fibers after removal of the FN cladding. We measured the electrical behavior of CNT fibers before and after removing the cladding. **Figure 5a** shows the representative data

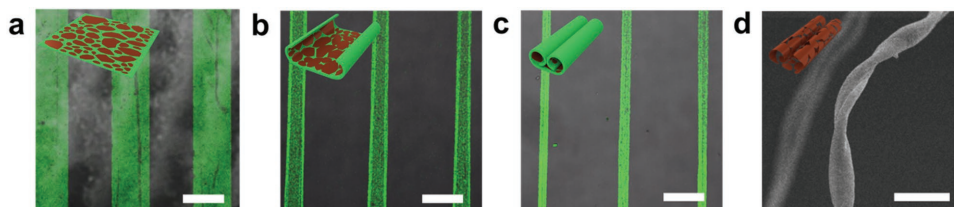


**Figure 2.** The time-dependent self-rolling process. a) GO sheets on a 100  $\mu\text{m}$  wide FN layer (green). b) GO sheets approach each other as the FN layer contracts. c) Dual tubular microstructure of the resulting FN/GO fiber. d) Removal of the FN cladding reveals the GO fiber (SEM image). Confocal fluorescence images were merged with DIC microscope images (a–c). Scale bars are 100  $\mu\text{m}$  for (a–c) and 50  $\mu\text{m}$  for (d).

for the CNT fibers that demonstrate the electrical conductivity ( $\approx 2 \times 10^{-2} \text{ S cm}^{-1}$ ), indicating that the originally dispersed CNT particles were physically connected when formed into millimeter-long CNT-based dual tubular fibers. Note that the conductivity of FN/CNT fibers was not measurable prior to removal of the FN cladding. In addition, the printed pattern of CNTs before the rolling process showed no electrical conductivity (Figure S3a, Supporting Information). These data suggest that contraction of the FN layer initiates formation of conductive fibers.

To disperse the graphene particles in an aqueous solution for the  $\mu\text{CP}$  process, they were initially oxidized, resulting in GOs which have a poor conductivity. After the GO microtubular fibers formed, chemical reduction of GO was required to obtain electrically conductive reduced graphene oxide (rGO) microtubular fibers (after removal of FN cladding).<sup>[28]</sup> The surface of

FN/GO microtubular fibers was examined with AFM at each step (Figure 5b). The dual tubular microstructure was clearly visible before and after removal of the FN cladding. Next, the GO microtubular fibers were reduced by exposing them to hydrazine vapor, and the fibers' surface was re-examined by AFM (Figure 5b). The image of the rGO fiber shows the morphology of microtubular fibers. To determine whether GO fibers reduced in hydrazine vapor retain rGO particles, we performed micro Raman spectroscopy on the fibers before and after the reduction process. The Raman spectra in Figure 5b (bottom right plot) show distinct peaks around 1352 and 1600  $\text{cm}^{-1}$  coinciding with the disorder-induced mode (D-band) and the tangential mode indicating the stacking structure in graphitic structures (G band), respectively.<sup>[28]</sup> The intensity ratio of these two bands (D/G) is often used to determine the average size of the in-plane  $\text{sp}^2$  domains. Due to the reduction process, which

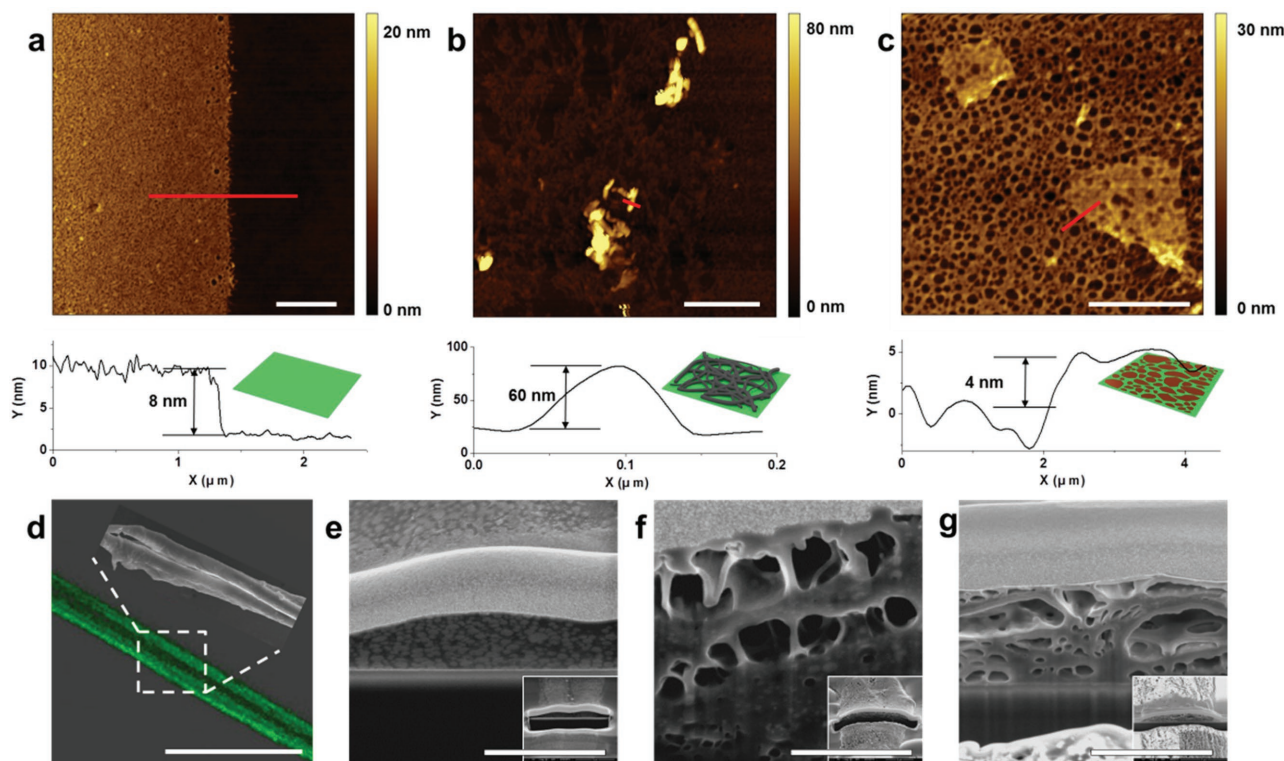


**Figure 3.** AFM images and line profiles (along with red line in AFM images) of a) an FN pattern, b) CNT particles on top of the FN pattern, and c) GO sheets on top of the FN pattern. d) 3D-reconstructed confocal image of FN/GO fibers using a 100  $\mu\text{m}$  wide FN pattern (green), and SEM image of the same. e–g) Focused ion beam cross-sectional SEM images of FN, FN/CNT, and FN/GO fibers (insets: low-magnification images). The length and diameter of used CNT are 1  $\mu\text{m}$  and 40–60 nm. Scale bars are 2  $\mu\text{m}$  for (a–c), 100  $\mu\text{m}$  for (d), 1  $\mu\text{m}$  for (e, g), and 500 nm for (f).

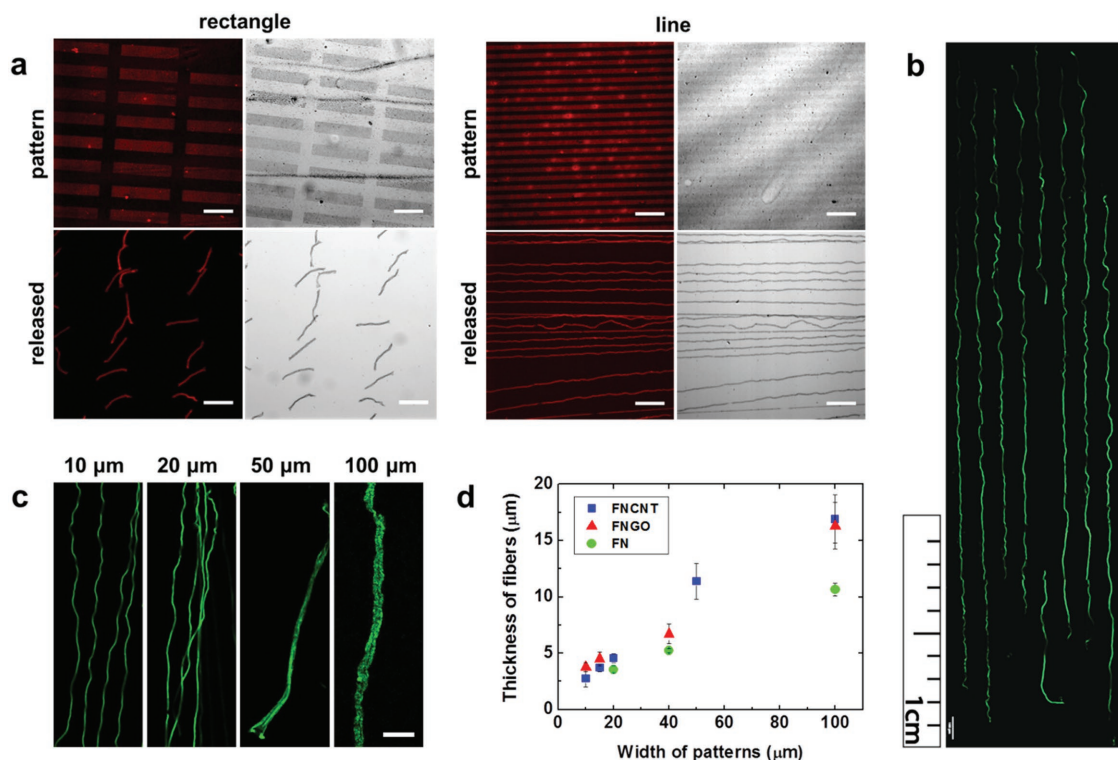


**Figure 4.** Features of composite fibers. a) Confocal microscope and bright field images of FN/CNT fibers using different sizes of FN patterns (red). b) Centimeter-long FN/GO fibers. c) FN/CNT fibers from FN line patterns have different widths. d) Graph of the thickness of fabricated composite fibers from different widths of FN patterns. Scale bars are 100 μm for (a), 1 cm for (b), and 50 μm for (c).

eliminates oxygen on the surface, rGO demonstrates graphite-like stacking, inducing a higher D/G ratio than that seen for GO. We observed a D/G ratio for rGO microtubular fibers of 1.170, which was higher than the 1.019 ratio observed for GO,

confirming the successful reduction of GO microtubular fibers. The red-shifted G peak of the rGO microtubular fiber (from 1607 to 1593  $\text{cm}^{-1}$ ) also indicates the recovery of  $\text{sp}^2$  domains on its surface (Figure S4, Supporting Information).<sup>[29,30]</sup>

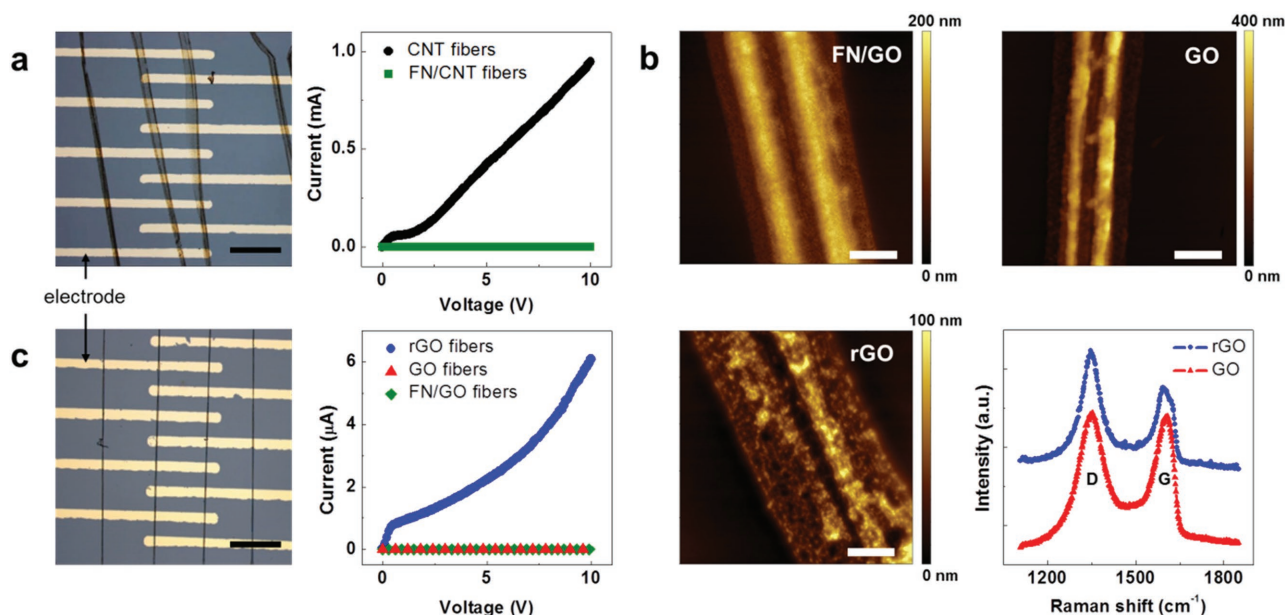


**Figure 5.** Characterization of fibers fabricated from carbon nanomaterials. a) Microscope image of gold electrodes on top of CNT fibers and their  $I$ - $V$  characteristics. b) AFM images of an FN/GO fiber, an FN-removed GO fiber, and a chemically reduced rGO fiber, and Raman spectra of GO and rGO fibers that confirm the reduction process. c) Gold electrodes on top of rGO fibers and their  $I$ - $V$  characteristics. Scale bars are 50 μm for (a, c) and 2 μm for (b).

Electrical conductivity was further confirmed for the fibers as shown in Figure 5c, indicating the successful removal of FN cladding and reduction of GO microtubular fibers to conductive rGO microtubular fibers. The electrical conductivity of the rGO microfiber was found to be  $\approx 1 \times 10^{-4} \text{ S cm}^{-1}$  (Figure 5c), while only negligible electrical conduction was observed with FN/GO and GO fibers (Figure S3b, Supporting Information).

To the best of our knowledge, this is the first report of a successful demonstration of the mass production of micrometer-to millimeter-scale fibrous architectures from carbon nanomaterials via soft lithography. Since this process allows patterning of virtually any type of nanomaterial, from metallic nanoparticles and nanowires to soft and biological materials, this could prove to be a universal method of translating nanomaterials to macroscale fibers. These highly extended or aligned fibrous nanostructures often offer high flexibility, or unexpected modulus, which is very difficult to fabricate with nanoscale building blocks. Although several alternative methods of manufacturing carbon fibers have been developed, such as electrospinning and mechanical yarning, our method is far simpler than any other reported methods.

In summary, we have fabricated millimeter-long carbon-based microtubular structures by inducing the strain-driven self-rolling of highly elastic protein layers. CNT and GO were used as core materials, and a soft and elastic ECM protein, FN, was used as an active layer to initiate the self-rolling process. This method is easy to perform and applicable to a wide variety of nanomaterials. Selective removal of the FN protein layer provided electrically conductive millimeter-long CNT and GO microtubules, which can be used to make carbon-based fabric devices. Solution dispersibility of the target nanomaterials is crucial for a successful  $\mu\text{CP}$  process. When this condition is met, the well-known technique of soft lithography allows widely varying dimensional architectures and homogeneity. During contraction, the dispersed fragments of printed carbon nanomaterials approximate, eventually forming a physically connected microtubular fiber. Electrical conduction through single microtubular fibers was confirmed, indicating that millimeter-scale fibers were successfully fabricated with nanoscale materials.

## Experimental Section

**Fabrication of Self-Rolling Fiber:** Sacrificial layer coated substrate was prepared by spin coating 10% (w/v) PIPAAm (Polysciences) in 1-butanol (Sigma-Aldrich) solution onto a glass coverslip. Two alternative water-dissolving materials, dextran (Sigma-Aldrich) and sucrose (Sigma), were dissolved in deionized water in the same concentration and spin coated onto a glass substrate after 20 min of UV-ozone treatment. Protein and carbon nanomaterials were patterned by double  $\mu\text{CP}$  using a polydimethylsiloxane (PDMS, Sylgard 184, Dow-Corning) stamp.  $\mu\text{CP}$  is generally used to produce microsize patterns on planar substrates. Patterns of various sizes and shapes were fabricated, including 10, 15, 20, 40, 50, and 100  $\mu\text{m}$  lines of various lengths ( $\mu\text{m}$  to cm scale). PDMS stamps were fabricated by a well-established soft lithography process.<sup>[31]</sup>

The first layer of FN (Gibco) was printed on a sacrificial layer. 50  $\mu\text{g mL}^{-1}$  FN in phosphate-buffered saline (PBS) solution was used as an ink, and 5  $\mu\text{g mL}^{-1}$  Alexa Fluor 488 or Alexa Fluor 555 (Alexa Fluor Succinimidyl Esters, Molecular probes, Life technologies) was added for fluorescence imaging. FN molecules in solution are globular dimers.

During incubation the dimers settled and stretched to an unfolded structure on the surface of the PDMS stamp. This prestrained layer was transferred from the hydrophobic PDMS surface to the less hydrophobic substrate. The second layer of carbon nanomaterials (CNT and GO) was printed on top of the FN layer. 0.15  $\text{mg mL}^{-1}$  CNT ink in a highly dispersed water-based solution with additional dispersant and a ball-milling process described in the previous paper were used and can be purchased from Lab311 in Korea.<sup>[32,33]</sup> GO solution (5  $\text{mg mL}^{-1}$ ) was purchased from Graphene Supermarket and diluted to 1  $\text{mg mL}^{-1}$  with deionized water. These carbon nanomaterials were also incubated on a PDMS stamp and transferred to the FN layer via the process used to transfer protein and carbon nanomaterials.

COOH-functionalized cadmium telluride QDs were purchased from Aldrich and dispersed in deionized water to a final concentration of 10  $\text{mg mL}^{-1}$ . AgNW suspended in 0.5% alcohol (Aldrich, 115  $\text{nm} \times 20\text{--}50 \mu\text{m}$ ) was diluted to 0.25% by adding the same volume of deionized water and sonicating for 30 min. AgNP solution was purchased from ANP Corporation in Korea (water-based ink) and diluted to 12.5% in deionized water. Fluorescent water-suspended amine-modified polystyrene (PS) beads of the following sizes were purchased from Aldrich: 1  $\mu\text{m}$  with red, 1  $\mu\text{m}$  with green, and 2  $\mu\text{m}$  with blue fluorescence. QD, AgNW, AgNP, and PS bead solutions were incubated and transferred to the FN layer via the process used to transfer protein and carbon nanomaterials.

The uncrosslinked PIPAAm layer was removed from the substrate by adding 40  $^{\circ}\text{C}$  hot water and cooling the water to below 32  $^{\circ}\text{C}$ . As the water cools down, PIPAAm polymer brushes form hydrogen bonds with water molecules, stretch, and dissolve. Dextran and sucrose layers were dissolved by adding water.

**Structural Analysis:** FN was stained with Alexa Fluor dyes for in situ observation of the rolling process via laser scanning confocal microscopy (710, Zeiss). Image contrast and brightness were enhanced using imageJ (National Institutes of Health). A 3D image was reconstructed from stacked images of self-rolled structures. For QD and fluorescent PS bead composite samples, FN was not labeled with fluorescent dye to permit accurate observation of QD and fluorescent PS beads inside fibers. The emission wavelength of QD was 510 nm. Dried samples were imaged by SEM (SNE-4500M, SEC and JSM 7600F, JEOL), allowing microstructural analysis of dual tubular fibers. High-resolution cross-sectional images of fabricated fibers were obtained using focused ion beam SEM (Helios NanoLab, FEI) to confirm the existence of carbon nanomaterials inside fibers. The thickness and morphology of micropatterns and fabricated fibers were analyzed using tapping mode AFM (PICOSTATION, SIS). Topographic images were used to quantify thickness and dimensions using the Gwyddion software (<http://gwyddion.net/>).

**Carbon Fibers:** Fine fibrous structures consisting of carbon nanomaterials (CNT and GO) were obtained after removing outer protein layers. FN cladding was removed by either 5 min of plasma treatment or 30 min in a 300  $^{\circ}\text{C}$  furnace in air.

**GO Reduction and Raman Spectroscopy:** GO solution was used, which is dissolved in water via hydrogen bonding between oxygen from GO and hydrogen from water molecules. GO is an insulator because it contains hydroxyl and epoxide groups, which disrupt  $\text{sp}^2$  bonding networks in graphene. Thus an additional chemical reduction process was required to obtain rGO fiber, which like graphene has good conductivity. Hydrazine monohydrate (Sigma-Aldrich) was used to produce hydrazine vapor at high temperature (100  $^{\circ}\text{C}$ , 1 h). Each reduction process was followed by AFM and Raman spectroscopy (Figure 5b). To produce GO fibers, the FN layer was removed from FN/GO fibers. The resulting GO fibers maintained the dual tubular microstructure of the FN/GO fibers, as confirmed by AFM. The chemical process of reduction was monitored by micro Raman spectroscopy, which is widely used to obtain structural information and detect defects, disorder, and doping in graphene and graphene-related materials.

**Conductivity Measurement:** To measure fiber conductivity, Ti/Au electrodes with a thickness of 5/30 nm were deposited on CNT and rGO fibers laid on a silicon wafer substrate. Electrodes were spaced 50  $\mu\text{m}$  apart. Because the FN cladding acts like an insulator to prevent

electrical contact between the electrodes and the fibers, conductivity was not able to measure in FN/CNT fibers. The  $I$ - $V$  curves of CNT and rGO fibers were measured three and seven times, respectively, and measured values were averaged. Conductivity was calculated by linearly fitting a line from the graph.

## Supporting Information

Supporting Information is available from the Wiley Online Library or from the author.

## Acknowledgements

This work was supported by the National Junior Research Fellowship Program (2014H1A8A1020296), the Leading Foreign Research Institute Recruitment Program (2013K1A4A3055268), and Mid-career Researcher Program (2016R1A2B3015239) funded by the Ministry of Science, ICT and Future Planning, Korea. T.L. and J.J. thank the financial support of the National Creative Research Laboratory program (2012026372) through the National Research Foundation of Korea.

## Conflict of Interest

The authors declare no conflict of interest.

## Keywords

carbon fibers, carbon nanotubes, fibronectin, graphene, strain-driven self-rolling

Received: March 28, 2017

Revised: April 29, 2017

Published online: June 19, 2017

- [1] S. J. Gerbode, J. R. Puzey, A. G. McCormick, L. Mahadevan, *Science* **2012**, *337*, 1087.
- [2] S. Armon, E. Efrati, R. Kupferman, E. Sharon, *Science* **2011**, *333*, 1726.
- [3] C. Dawson, J. F. V. Vincent, A.-M. Rocca, *Nature* **1997**, *390*, 668.
- [4] R. M. Erb, J. S. Sander, R. Grisch, A. R. Studart, *Nat. Commun.* **2013**, *4*, 1712.
- [5] B. Bar-On, X. Sui, K. Livanov, B. Achrai, E. Kalfon-Cohen, E. Wiesel, H. D. Wagner, *Appl. Phys. Lett.* **2014**, *105*, 033703.
- [6] L. Ionov, *Adv. Funct. Mater.* **2013**, *23*, 4555.
- [7] M. Takahashi, C. Figus, L. Malfatti, Y. Tokuda, K. Yamamoto, T. Yoko, T. Kitanaga, Y. Tokudome, P. Innocenzi, *NPG Asia Mater.* **2012**, *4*, e22.
- [8] I. S. Chun, X. Li, *IEEE Trans. Nanotechnol.* **2008**, *7*, 493.
- [9] X. Liu, J. Zhang, W. Si, L. Xi, B. Eichler, C. Yan, O. G. Schmidt, *ACS Nano* **2015**, *9*, 1198.
- [10] C. C. B. Bufon, J. D. C. González, D. J. Thurmer, D. Grimm, M. Bauer, O. G. Schmidt, *Nano Lett.* **2010**, *10*, 2506.
- [11] L. Ionov, *Mater. Today* **2014**, *17*, 494.
- [12] E. Palleau, D. Morales, M. D. Dickey, O. D. Velev, *Nat. Commun.* **2013**, *4*, 2257.
- [13] K. Malachowski, J. Breger, H. R. Kwag, M. O. Wang, J. P. Fisher, F. M. Selaru, D. H. Gracias, *Angew. Chem.* **2014**, *126*, 8183.
- [14] B. Yuan, Y. Jin, Y. Sun, D. Wang, J. Sun, Z. Wang, W. Zhang, X. Jiang, *Adv. Mater.* **2012**, *24*, 890.
- [15] R. Songmuang, C. Deneke, O. G. Schmidt, *Appl. Phys. Lett.* **2006**, *89*, 223109.
- [16] A. W. Feinberg, K. K. Parker, *Nano Lett.* **2010**, *10*, 2184.
- [17] L. F. Deravi, T. Su, J. A. Paten, J. W. Ruberti, K. Bertoldi, K. K. Parker, *Nano Lett.* **2012**, *12*, 5587.
- [18] A. W. Feinberg, A. Feigel, S. S. Shevkopylas, S. Sheehy, G. M. Whitesides, K. K. Parker, *Science* **2007**, *317*, 1366.
- [19] Y. Mei, G. Huang, A. A. Solovev, E. B. Ureña, I. Mönch, F. Ding, T. Reindl, R. K. Y. Fu, P. K. Chu, O. G. Schmidt, *Adv. Mater.* **2008**, *20*, 4085.
- [20] Y. Mao, J. E. Schwarzbauer, *Matrix Biol.* **2005**, *24*, 389.
- [21] E. P. S. Gee, D. E. Ingber, C. M. Stultz, *PLoS One* **2008**, *3*, e2373.
- [22] W. Lu, M. Zu, J.-H. Byun, B.-S. Kim, T.-W. Chou, *Adv. Mater.* **2012**, *24*, 1805.
- [23] L. Liu, W. Ma, Z. Zhang, *Small* **2011**, *7*, 1504.
- [24] Y. Dror, W. Salalha, R. L. Khalfin, Y. Cohen, A. L. Yarin, E. Zussman, *Langmuir* **2003**, *19*, 7012.
- [25] C. H. Kwon, S.-H. Lee, Y.-B. Choi, J. A. Lee, S. H. Kim, H.-H. Kim, G. M. Spinks, G. G. Wallace, M. D. Lima, M. E. Kozlov, R. H. Baughman, S. J. Kim, *Nat. Commun.* **2014**, *5*, 3928.
- [26] D. Zhang, M. Miao, H. Niu, Z. Wei, *ACS Nano* **2014**, *8*, 4571.
- [27] X. Li, P. Sun, L. Fan, M. Zhu, K. Wang, M. Zhong, J. Wei, D. Wu, Y. Cheng, H. Zhu, *Sci. Rep.* **2012**, *2*, 395.
- [28] D. R. Dreyer, S. Park, C. W. Bielawski, R. S. Ruoff, *Chem. Soc. Rev.* **2010**, *39*, 228.
- [29] S. Stankovich, D. A. Dikin, R. D. Piner, K. A. Kohlhaas, A. Kleinhammes, Y. Jia, Y. Wu, S. T. Nguyen, R. S. Ruoff, *Carbon* **2007**, *45*, 1558.
- [30] M. A. Khaderbad, V. Tjoa, T. Z. Oo, J. Wei, M. Sheri, R. Mangalampalli, V. R. Rao, S. G. Mhaisalkar, N. Mathews, *RSC Adv.* **2012**, *2*, 4120.
- [31] Y. Xia, G. M. Whitesides, *Angew. Chem., Int. Ed.* **1998**, *37*, 550.
- [32] O.-S. Kwon, H. Kim, H. Ko, J. Lee, B. Lee, C.-H. Jung, J.-H. Choi, K. Shin, *Carbon* **2013**, *58*, 116.
- [33] H. Ko, J. Lee, Y. Kim, B. Lee, C.-H. Jung, J.-H. Choi, O.-S. Kwon, K. Shin, *Adv. Mater.* **2014**, *26*, 2335.